High Repeatability of Quantitative Susceptibility Mapping (QSM) in the Head and Neck With a View to Detecting Hypoxic Cancer Sites

Anita Karsa[1], Shonit Punwani[2], and Karin Shmueli[1]
[1]*Department of Medical Physics and Biomedical Engineering, University College London, London, United Kingdom*
[2]*Centre for Medical Imaging, University College London, London, United Kingdom*

Synopsis

As hypoxic tumours in the head-and-neck are more resistant to radiation therapy, there is a pressing clinical need to measure tumour oxygenation non-invasively. Since deoxyhemoglobin in the blood, which indicates hypoxia, is paramagnetic, QSM is a candidate technique. Here, we tested QSM's repeatability in various head-and-neck regions in ten healthy volunteers to investigate the feasibility of detecting the susceptibility difference expected to result from hypoxia. We found low minimum detectable effect sizes in the lymph nodes (0.12 ppm), submandibular glands (0.08 ppm), and parotid glands (0.04 ppm). This high QSM repeatability paves the way for clinical studies.

Purpose

Tumour hypoxia is associated with adverse prognosis after radiotherapy (RT) in head-and-neck cancer[1]. Therefore, there is a pressing clinical need to measure tumour oxygenation and identify hypoxic sites to improve RT treatment. Blood deoxyhemoglobin, which increases in hypoxia[2], is paramagnetic[3] having higher susceptibility than surrounding tissues. QSM which calculates tissue magnetic susceptibility from MRI phase images[4-6] is a non-invasive method that could be useful to measure tissue oxygenation. Here we measured the repeatability of a QSM protocol optimised for the head-and-neck to determine whether QSM is stable enough to detect hypoxic sites in this region.

Methods

Multi-echo head-and-neck images were acquired in 10 healthy volunteers at 3T (Achieva, Philips Healthcare, NL) using a 16-channel head-and-neck RF coil and an optimised 3D gradient-echo sequence[7,8] (Figure 1a). All volunteers were scanned 3 times per session at two sessions a week apart to investigate both intrasession and intersession repeatability. Head-and-neck tissue masks were generated by thresholding the inverse noise map[9-10]. An optimised QSM pipeline was applied: 1. Non-linear field fitting[11], 2. Laplacian phase unwrapping[12], 3. Projection onto Dipole Fields[13], 4. Iterative fitting in image space with Tikhonov regularisation[10] with regularisation parameter $\alpha = 0.11$ and correction for susceptibility underestimation[12].

In the first acquired images of each volunteer, brain regions (Figure 1b) were automatically segmented (Figure 2) using FSL FIRST[14] on the first-echo magnitude images, and neck regions of interest (ROIs) (Figure 1b) were manually delineated using ITK- SNAP[15-16]. Regions were checked by an experienced radiologist (Figure 2). ROIs in the remaining five images were delineated using segmentation propagation: the last-echo magnitude image of the first scan was non-rigidly registered[17-19] to the rest of the last-echo magnitude images and the resulting transformations were used to warp the segmented ROIs. All ROIs were checked visually and manually adjusted if necessary (Figure 2).

Mean and median susceptibilities were calculated in all ROIs. The distributions of the susceptibility differences measured between scans were used to assess intrasession and intersession repeatability for each ROI. The minimum detectable effect size[20] (MDE) was calculated for each ROI based on the standard deviation of the corresponding distribution with type I and II error rates of $\alpha = 0.05$ and $\beta = 0.2$ respectively.

Results and Discussion

Figure 3 shows the distributions of intrasession and intersession median susceptibility differences for each ROI. Most of the distributions are centered around zero (within 0.02 ppm) except those of the GP (the ROI abbreviations can be found in Figure 1b). This could be because the GP has a much higher susceptibility than the surrounding tissue, therefore inaccuracies in its segmentation can lead to bigger, systematic errors. The intersession distribution in mN is also substantially further off-center than the rest. This could be because intersession co-registration was often inaccurate due to the mN's relatively small size and they were usually surrounded by much more paramagnetic fatty tissue[8]. lNs were larger and were, therefore, segmented with a 2 mm margin on each side mitigating the effects of inaccurate segmentation and leading to much higher repeatability (narrower distribution with a center closer to zero).

Brain regions had higher repeatability and, consequently, smaller MDEs (Figure 4) than neck regions. The intrasession repeatability was always greater than or equal to the intersession repeatability for each region, especially for the SMg where the intersession MDE was double that of the intrasession MDE. This may have been because of positioning, physiological or system differences. Susceptibility of the Pg had especially high intrasession and intersession repeatability. All MDEs were lower than 0.2 ppm. Results based on the mean susceptibility (not shown) were almost identical in these healthy volunteers.

The susceptibility difference between fully oxygenated and fully deoxygenated blood[3] is $\Delta\chi_{blood} = Hct \cdot 3.8\,ppm$, where Hct is the hematocrit. Therefore, the susceptibility difference between hypoxic and normoxic sites can be estimated as $\chi_{hypoxic} - \chi_{normoxic} = V \cdot \Delta\chi_{blood}$, where V denotes the vascular density. Substituting $Hct = 0.4$ and $V = 0.2$, which are

both realistic values for healthy and cancerous tissue[21-24], the susceptibility difference is about 0.3 ppm which is substantially higher than the measured MDEs. Note that the exact susceptibility difference scales linearly with V which was approximated to be higher (0.85) by Panek et al.[25]

Conclusions

Susceptibility values measured in healthy lymph nodes, large nodular structures, and the parotid and submandibular glands had sufficient repeatability to enable future detection of the estimated susceptibility difference between normoxic and hypoxic tissue. Therefore, QSM could potentially identify hypoxic sites in head-and-neck cancer. Careful delineation of ROIs is crucial to avoid inaccuracies, especially if the susceptibility difference between the region and its surroundings is high, e.g. for healthy lymph nodes embedded in paramagnetic fatty fascia.

1. Nordsmark, Marianne, et al. "Prognostic value of tumor oxygenation in 397 head and neck tumors after primary radiation therapy. An international multi-center study." *Radiotherapy and Oncology* 77.1 (2005): 18-24.
2. Baudelet, Christine, and Bernard Gallez. "How does blood oxygen level-dependent (BOLD) contrast correlate with oxygen partial pressure (pO2) inside tumors?" *Magnetic resonance in medicine* 48.6 (2002): 980-986.
3. Jain, Varsha, et al. "Investigating the magnetic susceptibility properties of fresh human blood for noninvasive oxygen saturation quantification." *Magnetic resonance in medicine* 68.3 (2012): 863-867.
4. Shmueli, Karin, et al. "Magnetic susceptibility mapping of brain tissue in vivo using MRI phase data." *Magnetic resonance in medicine* 62.6 (2009): 1510-1522.
5. Reichenbach, J. R., et al. "Quantitative susceptibility mapping: concepts and applications." *Clinical neuroradiology* 25.2 (2015): 225-230.
6. Eskreis-Winkler, Sarah, et al. "The clinical utility of QSM: disease diagnosis, medical management, and surgical planning." *NMR in Biomedicine* 30.4 (2017).
7. Karsa, A., Punwani, S., & Shmueli, K. “The effect of low resolution and coverage on the accuracy of susceptibility mapping.” *Magnetic Resonance in Medicine* (2018).
8. Karsa, Anita, et al. “Fat Correction of MRI Phase Images for Accurate Susceptibility Mapping in the Head and Neck.” *In Proceedings of the 25th Annual Meeting of the ISMRM, Paris* (2018): p. 4988
9. MEDI toolbox: http://weill.cornell.edu/mri/pages/qsm.html
10. Kressler, Bryan, et al. "Nonlinear regularization for per voxel estimation of magnetic susceptibility distributions from MRI field maps." *IEEE transactions on medical imaging* 29.2 (2010): 273.
11. Liu, Tian, et al. "Nonlinear formulation of the magnetic field to source relationship for robust quantitative susceptibility mapping." *Magnetic resonance in medicine* 69.2 (2013): 467-476.
12. Schweser, Ferdinand, et al. "Toward online reconstruction of quantitative susceptibility maps: superfast dipole inversion." *Magnetic resonance in medicine* 69.6 (2013): 1581-1593.
13. Liu, Tian, et al. "A novel background field removal method for MRI using projection onto dipole fields." *NMR in Biomedicine* 24.9 (2011): 1129-1136.
14. Patenaude, Brian, et al. "A Bayesian model of shape and appearance for subcortical brain segmentation." *Neuroimage*56.3 (2011): 907-922.
15. Yushkevich, Paul A., et al. "User-guided 3D active contour segmentation of anatomical structures: significantly improved efficiency and reliability." *Neuroimage* 31.3 (2006): 1116-1128.
16. ITK-SNAP: www.itksnap.org
17. Rueckert, Daniel, et al. "Nonrigid registration using free-form deformations: application to breast MR images." *IEEE transactions on medical imaging* 18.8 (1999): 712-721.
18. Lee, Seungyong, George Wolberg, and Sung Yong Shin. "Scattered data interpolation with multilevel B-splines." *IEEE transactions on visualization and computer graphics* 3.3 (1997): 228-244.
19. MATLAB b-spline: https://uk.mathworks.com/matlabcentral/fileexchange/20057-b-spline-grid-image-and-point-based-registration
20. Bloom, Howard S. "Minimum detectable effects: A simple way to report the statistical power of experimental designs." *Evaluation review* 19.5 (1995): 547-556.
21. Weisskoff, Robert M., and Suzanne Kiihne. "MRI susceptometry: image-based measurement of absolute susceptibility of MR contrast agents and human blood." *Magnetic resonance in medicine* 24.2 (1992): 375-383.
22. Fein, Douglas A., et al. "Pretreatment hemoglobin level influences local control and survival of T1-T2 squamous cell carcinomas of the glottic larynx." *Journal of Clinical Oncology* 13.8 (1995): 2077-2083.
23. Seda, C. J., et al. "Thrombocytosis and hematocrit as prognostic factors in renal carcinoma." *Arch Esp Urol* 64.9 (2011): 883-890.
24. Dewhirst, Mark W., et al. "Morphologic and hemodynamic comparison of tumor and healing normal tissue microvasculature." *International Journal of Radiation Oncology• Biology• Physics* 17.1 (1989): 91-99.
25. Panek, R., Welsh, L., Dunlop, A., Wong, K.H., Riddell, A.M., Koh, D.M., Schmidt, M.A., Doran, S., Mcquaid, D., Hopkinson, G. and Richardson, C. “Repeatability and sensitivity of T_2* measurements in patients with head and neck squamous cell carcinoma at 3T.” *Journal of Magnetic Resonance Imaging*, 44(1), (2016): 72-80

a) Acquisition parameters	
Sequence	3D GRE
Coil	16-channel head-and-neck coil
Field-of-view	24 cm × 24 cm × 144 cm
Orientation	Coronal
SENSE factor	2 (right-left)
Resolution	1.25 mm isotropic
TE_1	4.61 ms (in-phase)
ΔTE	4.61 ms
Number of echoes	4
TR	22 ms
Flip angle	12°
Flow compensation	ON

b) Regions of interest (ROIs)	
In the brain	**In the neck**
Thalamus (**Thal**)	Medium-sized lymph nodes (**mN**) with a short axis diameter >4 mm
Caudate nucleus (**CN**)	Large nodular structures (**INs**) segmented by leaving a 2 mm margin on each side
Putamen (**Put**)	Parotid gland (**Pg**)
Globus pallidus (**GP**)	Submandibular gland (**SMg**)

Figure 1: MRI acquisition parameters (a) and regions of interest (b).

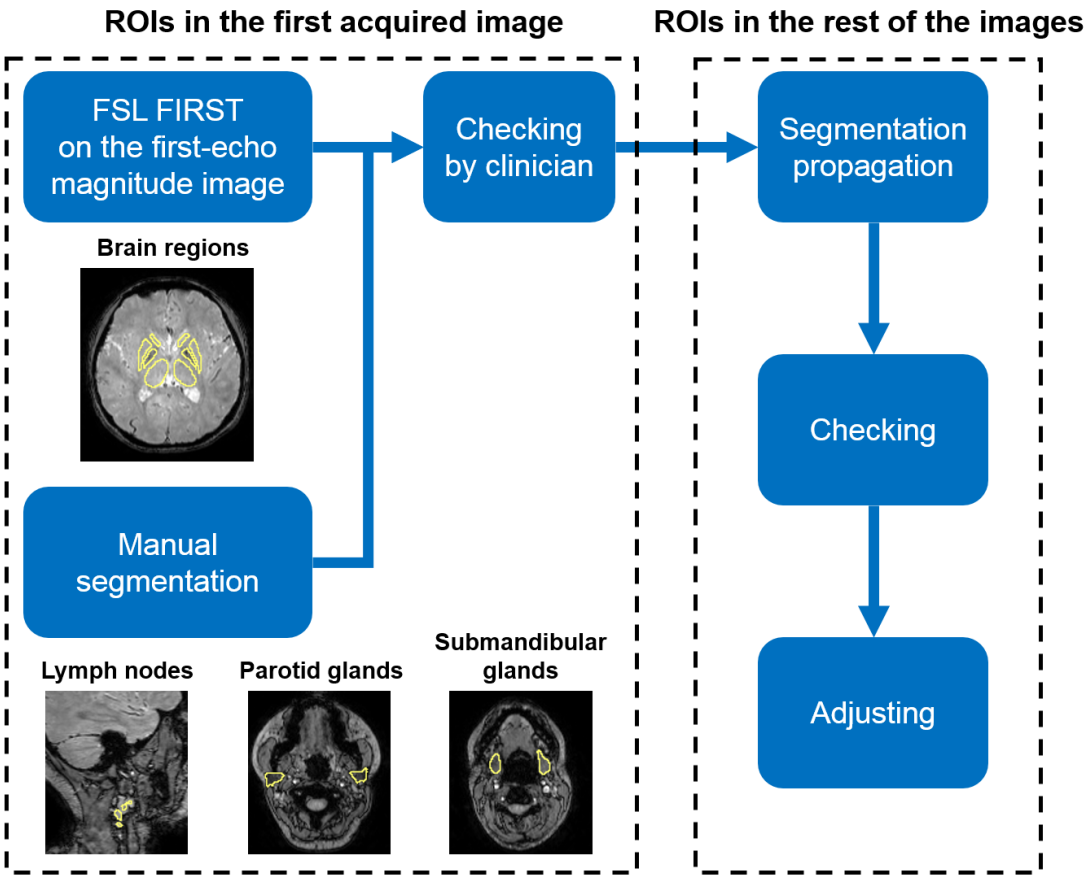

Figure 2: Pipeline for segmenting regions of interest in the brain and the head-and-neck tissues. The example ROIs are overlaid on the last-echo magnitude images.

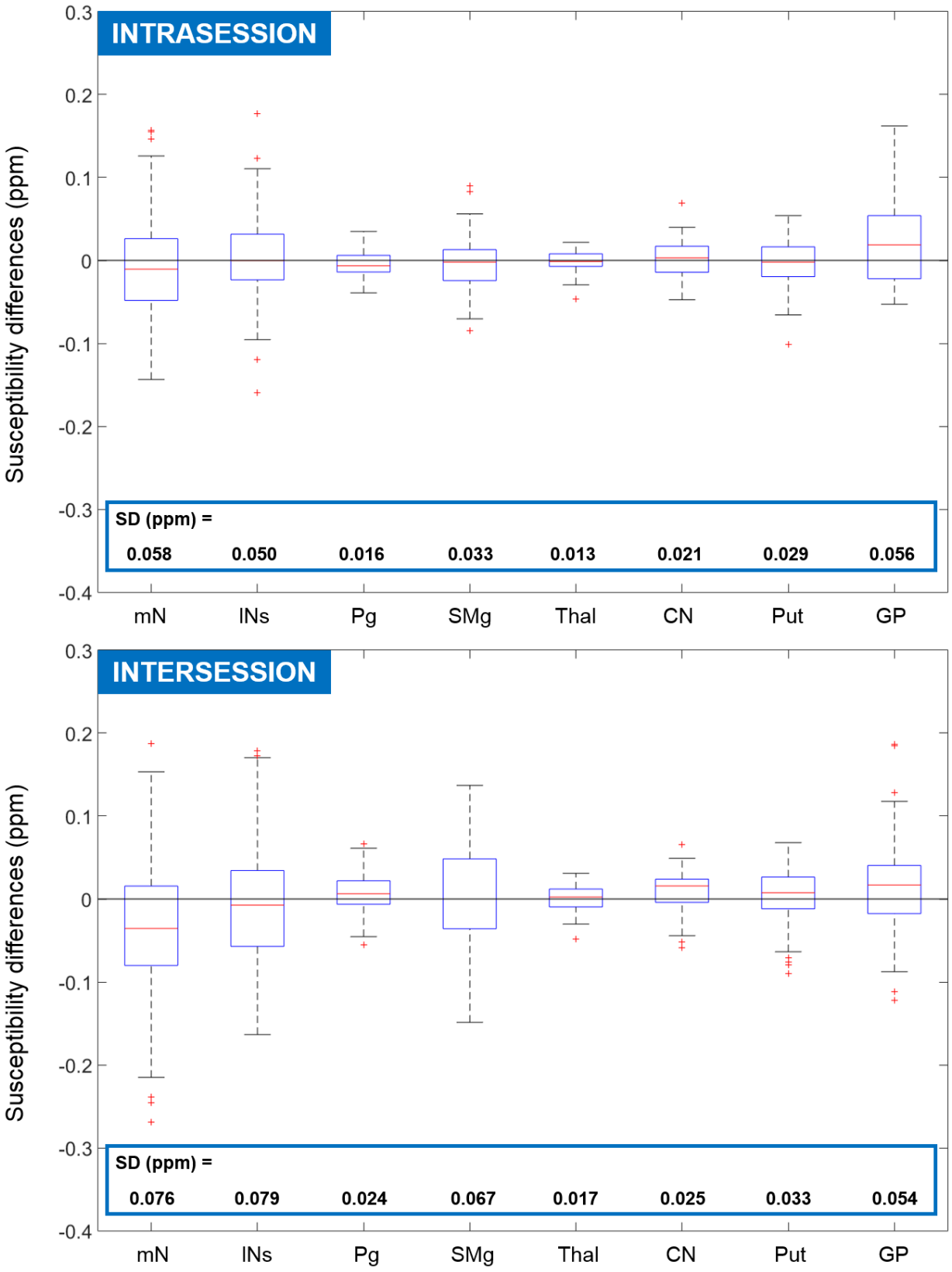

Figure 3: Box plots of intrasession (top) and intersession (bottom) median susceptibility differences in different ROIs: mN – medium-sized lymph nodes (short-axis diameter > 5 mm), lNs – large nodular structures (segmented with a 2 mm margin), Pg – parotid gland, SMg – submandibular gland, Thal – thalamus, CN – caudate nucleus, Put – putamen, GP – globus pallidus. Standard deviations (SD) of each distribution are displayed at the bottom of both plots. Box plots of the mean susceptibility differences were very similar (not shown).

Region of interest	Intrasession MDE (ppm)	Intersession MDE (ppm)
Medium-sized lymph nodes (mN)	0.144	0.189
Large nodal structures (lNs)	0.124	0.196
Parotid gland (Pg)	0.040	0.060
Submandibular gland (SMg)	0.082	0.166
Thalamus (Thal)	0.032	0.042
Caudate nucleus (CN)	0.052	0.062
Putamen (Put)	0.072	0.082
Globus pallidus (GP)	0.139	0.134

Figure 4: Minimum detectable effect sizes (MDE) calculated for each ROI from the intrasession and intersession standard deviations of median susceptibility differences. MDEs based on mean susceptibility differences were very similar (not shown).